The Astrophysical Journal, 815:20 (7pp), 2015 December 10 doi:10.1088/0004-637X/815/1/20
© 2015. The American Astronomical Society. All rights reserved.

INTERSTELLAR FLOW LONGITUDE FROM THE SYMMETRY OF THE PICKUP ION CUTOFF AT 1 AU

E. Möbius[1], M. A. Lee[1], and C. Drews[2]
[1] Space Science Center & Department of Physics, University of New Hampshire, Durham, NH, USA
[2] Institut für Experimentelle und Angewandte Physik, Christian-Albrecht-Universität, Kiel, Germany
Received 2015 September 28; accepted 2015 November 1; published 2015 December 2

ABSTRACT

We provide a proof of concept that the pickup ion (PUI) cutoff speed variation with ecliptic longitude can provide the interstellar neutral (ISN) flow longitude $\lambda_{\mathrm{ISN}\infty}$ outside the heliosphere with a precision of the order of $0\overset{\circ}{.}1$. We compare 2007–2014 *STEREO A* PLASTIC observations in the solar wind frame with a simple analytical cutoff model and perform a Pearson correlation of the cutoff as a function of longitude with those values mirrored about a location λ_{M} that slides in longitude. The resulting maximum correlation at $\lambda_{\mathrm{M}} = 255\overset{\circ}{.}21 \pm 0\overset{\circ}{.}04$ reflects the ISN upwind direction with a purely statistical uncertainty. This result is consistent with recent ISN flow longitude values, but a precision determination requires the evaluation of underlying systematic effects. Obtaining a precision ISN flow longitude is highly complementary to the *IBEX* ISN observations, which return a narrow tube in the ISN parameter space that couples flow speed and longitude tightly, but leaves a substantially larger error bar along the tube. The ISN flow provides one cardinal axis of the heliosphere, with a strong leverage on the plane subtended by the ISN velocity and the interstellar magnetic field vector, which controls the shape of the heliosphere and its interaction with the interstellar medium. In addition, a discussion about potential temporal variations of the ISN flow has started. Both issues require a precision determination of the ISN flow velocity over decade-long time intervals. *ACE* SWICS, *STEREO* PLASTIC, and *SOHO* CTOF PUI data allow such long-term studies over almost two decades.

Key words: ISM: atoms – ISM: kinematics and dynamics – local interstellar matter – solar wind – Sun: heliosphere

1. INTRODUCTION

Over the past decade the outer frontier of the heliosphere and the local interstellar medium have entered the spotlight of heliophysics research with the *Voyagers* at the heliopause and *IBEX* providing a simultaneous global view of the boundary region and sampling the interstellar neutral (ISN) gas flow. Together with global heliospheric modeling, which has been growing tremendously in sophistication and realism, these observations have revolutionized our picture of the heliosphere. One key quantity that controls the global interstellar medium–heliosphere interaction is the velocity vector of the Local Interstellar Cloud (LIC) relative to the Sun. This velocity vector, along with the LIC temperature, has been the objective of numerous studies, starting with UV backscatter observations of H (Bertaux & Blamont 1971; Thomas & Krassa 1971; Adams & Frisch 1977) and He (Weller & Meier 1974; Ajello 1978), followed by pickup ion (PUI) detection (Möbius et al. 1985; Gloeckler et al. 1992), and direct measurements of ISN He (Witte et al. 1996).

In an attempt to consolidate the local interstellar parameters (Gloeckler et al. 2004; Lallement et al. 2004; Möbius et al. 2004; Witte 2004) with all available observation techniques, the authors noted that the direct ISN imaging potentially provides the most detailed determination of the ISN flow vector and temperature, albeit at that time solely for He. The direct H, He, O, and Ne ISN observations (Möbius et al. 2009, 2012; Bochsler et al. 2012; Saul et al. 2012) provide new information with expanded species coverage and a vastly increased signal to background ratio. These measurements lead to a very precise relation between ISN flow longitude and speed via the hyperbolic trajectory equation, but the uncertainty in the longitude or speed separately is much larger (Bzowski et al. 2012, 2015; McComas et al. 2012, 2015a; Möbius et al. 2012, 2015b; Leonard et al. 2015) because of the limited longitude range of the *IBEX* observations, as illustrated in the compilation of ISN flow vector results by Schwadron et al. (2015) in Figure 1. While the uncertainties can be reduced with additional observations and a variation in the *IBEX* pointing strategy (Möbius et al. 2015a), there will always be a larger uncertainty along the ISN parameter tube if based solely on *IBEX* observations. Thus, an independent determination of the ISN longitude, as indicated by the vertical bar in Figure 1, will substantially tighten the determination of the flow vector in combination with further narrowing of the *IBEX* parameter tube through a growing database.

The ISN flow vector is one key hinge point that determines the shape of the heliopause and the interaction of the interstellar plasma in the outer heliosheath with the ISN flow. The second hinge point is the interstellar magnetic field direction, which is deduced from the orientation of the *IBEX* ribbon, consistent with the heliospheric asymmetry found by the *Voyagers* (Opher et al. 2007; Pogorelov et al. 2009) and the TeV cosmic ray anisotropy (Schwadron et al. 2014). In combination, the ISN flow and the magnetic field vector define the so-called *B–V* plane, which determines the symmetry of the outer heliosheath. In addition, a debate about possibly detectable temporal variations of the ISN flow vector has started (Frisch et al. 2013, 2015; Lallement & Bertaux 2014). To detect such variations, or to place tight upper limits on them, requires the precise determination of the ISN flow vector over an extended time span of more than one decade.

The needed independent information about the ISN flow longitude can be derived from the characteristic ISN flow structures in the inner heliosphere, i.e., the gravitational focusing cone (Möbius et al. 1995; Gloeckler et al. 2004) and the crescent, both identifiable with PUI observations at 1 AU (Drews et al. 2012). Although remarkably resilient to solar wind structures and potential sensor efficiency variations,

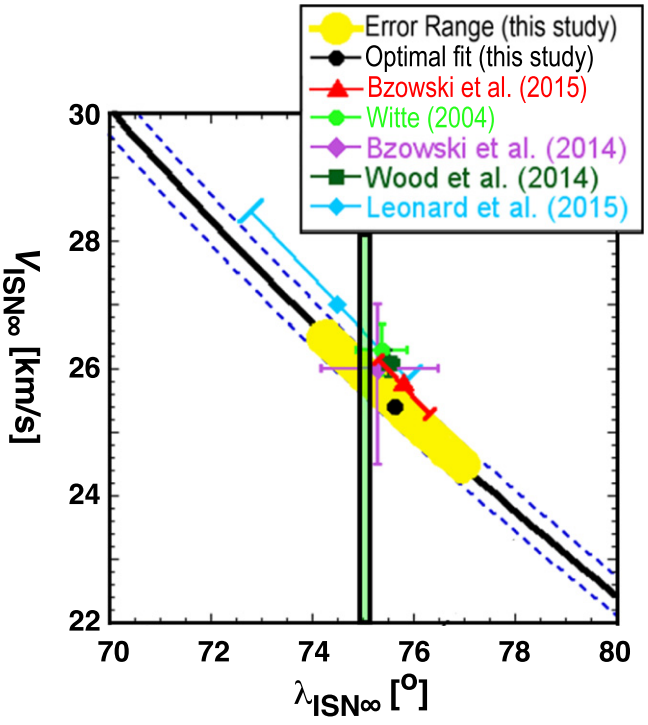

Figure 1. Relationship between $V_{\mathrm{ISN}\infty}$ and $\lambda_{\mathrm{ISN}\infty}$ according to the *IBEX* parameter tube based on various *IBEX* analyses in comparison with Ulysses results (adapted from Schwadron et al. 2015). Also shown with a vertical bar is how an independent measurement of $\lambda_{\mathrm{ISN}\infty}$ will constrain the ISN flow vector.

which have been eliminated in a careful statistical study by Drews et al. (2012), spatial and temporal variations of the ionization rate (Sokol & Bzowski 2014) and PUI transport effects (Möbius et al. 1996; Chalov & Fahr 2006; Chalov 2014) may lead to subtle deviations of the PUI spatial distribution relative to the parent neutral gas structures. A more robust independent observation may draw on the finding by Möbius et al. (1999) that the cutoff speed of the interstellar PUI distribution reflects the variation of the radial velocity component of the ISN flow at 1 AU with ecliptic longitude and thus is an indicator of the ISN flow longitude.

In this paper we present a proof of concept of how the variation of the PUI cutoff shift with ecliptic longitude can be used to determine the longitude of the ISN flow vector outside the heliosphere. We present the methodology in Section 2 and the preliminary analysis of *STEREO A* PLASTIC observations in Section 3. Section 4 contains a discussion of the results, and their ramifications and applications, followed by a brief conclusion and outlook on how such an analysis can draw on existing multi-year and multi-spacecraft observations at 1 AU.

2. DETERMINATION OF THE PUI CUTOFF SHIFT AND RELATED ANALYSIS METHODS

As shown by Möbius et al. (1999) the interstellar PUI cutoff speed is a function of the ratio of the radial ISN flow component and the solar wind speed at the observer location. The radial flow component V_r is largest precisely upwind and decreases symmetrically as the angle $|\lambda|$ increases, where $\lambda = \lambda_{\mathrm{Obs}} - \lambda_{\mathrm{ISN}\infty} - 180°$ and λ_{Obs} is the longitude of the observer. The PUI distribution is typically represented in terms of the PUI speed V_{PUI} normalized to the solar wind speed V_{sw} as $w = V_{\mathrm{PUI}}/V_{\mathrm{SW}}$. Assuming that any initial modification of the PUI distribution due to waves propagating along the magnetic field at the Alfvén speed is negligible and realizing that the spacecraft motion with the Earth is perpendicular to the radial direction, to a good approximation the normalized PUI cutoff speed in the solar wind frame (primed variable) is

$$w'_{\mathrm{CutOff}} = \frac{V_{\mathrm{SW}} + V_r}{V_{\mathrm{SW}}}, \tag{1}$$

where $V_r(\lambda, V_{\mathrm{ISN}\infty})$ is a function of λ and the ISN flow speed at infinity $V_{\mathrm{ISN}\infty}$.

The ISN bulk velocity at 1 AU as a function of λ is derived by considering the hyperbolic trajectory of an atom of mass m, whose speed at large distances is $V_{\mathrm{ISN}\infty}$, using polar coordinates (R, θ) centered at the Sun in the plane normal to its (constant) angular momentum $\boldsymbol{l}$, which in terms of the azimuthal velocity component V_θ satisfies $l = |\boldsymbol{l}| = mR\,|V_\theta|$:

$$\frac{1}{R} = \frac{m^2 G M_S}{l^2}(1 + \varepsilon \cos\theta). \tag{2}$$

G is the gravitational constant, M_s is the solar mass, and ε is the orbit eccentricity with $\varepsilon^2 = 1 + l^2 V_{\mathrm{ISN}\infty}^2 (GmM_S)^{-2}$ (Lee et al. 2012, 2015). Since the ISN bulk velocity vector lies within ~5° of the ecliptic plane, we may assume that the orbital plane is equivalent to the ecliptic plane. Using dimensionless quantities based on Earth's orbit (assumed circular) of radius R_{E} with speed V_{E}, $v = V/V_{\mathrm{E}}$ and $r = R/R_{\mathrm{E}}$, we obtain

$$\varepsilon^2 = 1 + r^2 v_\theta^2 v_{\mathrm{ISN}\infty}^2. \tag{2a}$$

Although l and ε are constants along the orbit, their values vary with λ and must be calculated along with the atom velocity. From Equation (2) we note that $\cos\theta_\infty = -\varepsilon^{-1}$, where θ_∞ is the "true anomaly," which is the angle swept out as the atom moves from infinity to perihelion. When the atom arrives at 1 AU ($r = 1$), evidently $\theta = \theta_\infty - |\lambda|$. Inserting this condition into Equation (2), as well as using Equation (2*a*) and the dimensionless quantities, we obtain

$$v_\theta^2 - |v_\theta| v_{\mathrm{ISN}\infty} \sin|\lambda| - (1 - \cos\lambda) = 0. \tag{3}$$

The solution of Equation (3) is

$$|v_\theta| = \left\{ v_{\mathrm{ISN}\infty} \cdot \sin|\lambda| + \left[v_{\mathrm{ISN}\infty}^2 \cdot \sin^2\lambda + 4(1 - \cos\lambda) \right]^{1/2} \right\} \Big/ 2. \tag{4}$$

Employing $v^2(r) = v_r^2(r) + v_\theta^2(r)$ and conservation of energy with $v^2(r)|_{r=1\,\mathrm{AU}} = v_0^2 = v_{\mathrm{ISN}\infty}^2 + 2$, we obtain

$$v_r^2 = 2 + v_{\mathrm{ISN}\infty}^2 - (1 - \cos\lambda) - \left\{ v_{\mathrm{ISN}\infty}^2 \sin^2\lambda + v_{\mathrm{ISN}\infty} \times \sin|\lambda| \left[v_{\mathrm{ISN}\infty}^2 \sin^2\lambda + 4(1 - \cos\lambda) \right]^{1/2} \right\} \Big/ 2. \tag{5}$$

At the ecliptic longitude λ_0, where the ISN bulk flow reaches its perihelion at 1 AU (Lee et al. 2012, 2015), we find $\cos\lambda_0 = -(1 + v_{\mathrm{ISN}\infty}^2)^{-1}$ and $v_r = 0$. For the case $|\lambda| < |\lambda_0|$ we have $v_r < 0$ and for the case $|\lambda| > |\lambda_0|$ we have $v_r > 0$.

Figure 2 shows schematically how the addition of the ISN flow velocity to the initial PUI velocity determines the value of w'_{CutOff} as a function of longitude. Shown are the ISN trajectory that arrives exactly from the upwind direction (top-right) and the one, for which the perihelion distance is at 1 AU

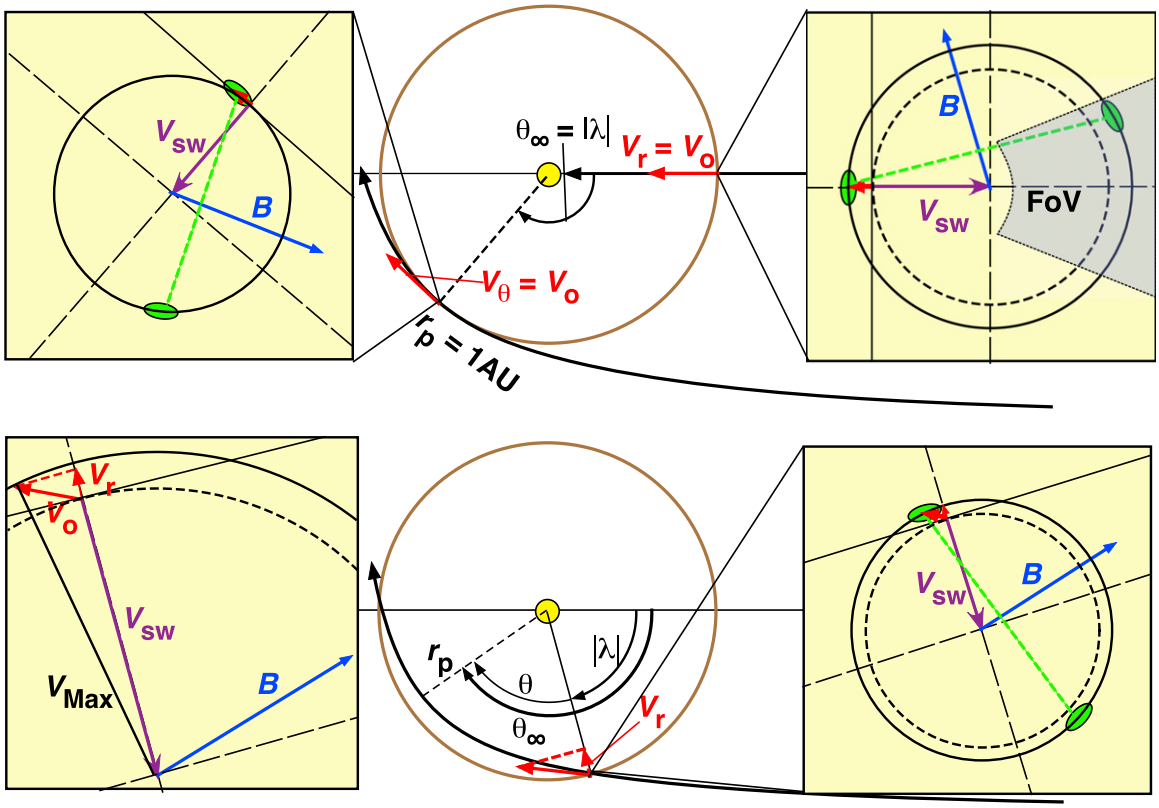

Figure 2. Schematic view of ISN flow trajectories with varying angular momenta and resulting radial V_r and tangential V_θ velocity components at various longitudes λ from the upwind direction. Top: exactly upwind and where the ISN flow is exactly tangential to the Earth's orbit. Bottom: arbitrary location between the former two. The insets on the upper left and right and the lower right show a cut through the resulting PUI velocity distribution in the plane that contains $\boldsymbol{V}_{\rm SW}$ and $\boldsymbol{B}$ in the solar wind frame, showing the initial ring-beam distribution upon injection at the combined solar wind and ISN flow velocity for a magnetic field direction so that the ring-beam is fully in the *STEREO* PLASTIC FOV (top right). The dashed circle indicates the edge of the PUI distribution for $V_r = 0$. The blow-up in the lower left shows how the velocity components add up to the maximum PUI speed $V_{\rm Max}$.

(top-left). In the lower panel is shown an arbitrary trajectory that crosses 1 AU. The ISN velocity at 1 AU is exactly radial ($v_r = v_o$) in the upwind direction and exactly tangential ($v_\theta = v_o$) for the trajectory with its perihelion distance $r_p = 1$ AU. For any arbitrary trajectory both velocity components are nonzero. Also included are the angles λ, θ, and θ_∞. The insets that are connected to the 1 AU crossing points of the trajectories (right and left in the top panel and right in the bottom panel) show how the combination of the solar wind velocity $\boldsymbol{V}_{\rm SW}$ and the local ISN flow velocity $\boldsymbol{V}_o$ translates into the speed of the outermost shell of the PUI distribution in velocity space in the solar wind frame for a cut in the plane that contains $\boldsymbol{V}_{\rm SW}$ and the interplanetary magnetic field (IMF) $\boldsymbol{B}$ (blue). Also shown is the cut through the initial ring-beam distribution (green) for $\boldsymbol{B}$ at an oblique angle relative to $\boldsymbol{V}_{\rm SW}$ that is identical in all three cases. It becomes obvious that the PUI speed of the outermost shell $V_{\rm Max}$, which determines $w_{\rm CutOff}$, arises from a vector addition of $\boldsymbol{V}_{\rm SW}$ and $\boldsymbol{V}_o$. However, as can be seen from the blow-up of the situation for the arbitrary trajectory in the lower left inset, clearly the main contribution of the ISN flow velocity to $V_{\rm Max}$ comes from V_r, and under any configuration the contribution from V_θ is smaller by about one order of magnitude based on the ratio $V_0/V_{\rm SW}$, which is typically of the order $1/10$. Exactly upwind and downwind (only shown for the upwind situation) the results when only including V_r are exact. Therefore, using just V_r as in Möbius et al. (1999) and in this study appears sufficient, particularly in view of the fact that we will only need to determine the symmetry line of the variation of $w_{\rm CutOff}$ in order to find the ISN flow longitude $\lambda_{\rm ISN\infty}$, as we will discuss in detail in Section 3. It is the symmetry that we will exploit with PUI observations from *STEREO A* PLASTIC in the following to demonstrate that these observations can be used toward an accurate determination of $\lambda_{\rm ISN\infty}$.

3. PRELIMINARY ANALYSIS OF THE PUI CUTOFF OBSERVED BY *STEREO A*

When evaluating the cutoff speed of the PUI distributions observed with *Solar and Heliospheric Observatory* (*SOHO*) CELIAS CTOF and with AMPTE SULEICA, Möbius et al. (1999) determined the cutoff values $w_{\rm CutOff}$ in the sunward facing sector (only sector available with CTOF) in the spacecraft frame. This method returns accurate values for the cutoff speed $w'_{\rm CutOff}$ in the solar wind frame, or exactly the maximum PUI injection speed $V_{\rm Max}$, only in the case of immediate pitch angle scattering when an isotropic PUI distribution forms quickly after injection. However, it has been shown that incomplete scattering leads to anisotropies in the PUI distribution (Gloeckler et al. 1995) and strong smoothing of the cutoff (Möbius et al. 1998). First, Oka et al. (2002) showed that the original ring-beam distribution may be maintained for some time after injection, and recently, Drews et al. (2015) confirmed that such ring-beam distributions are indeed a common feature of interstellar He PUI distributions in the inner heliosphere. As can be gleaned from Figure 2, a PUI ring-beam distribution (indicated in green in the insets) will

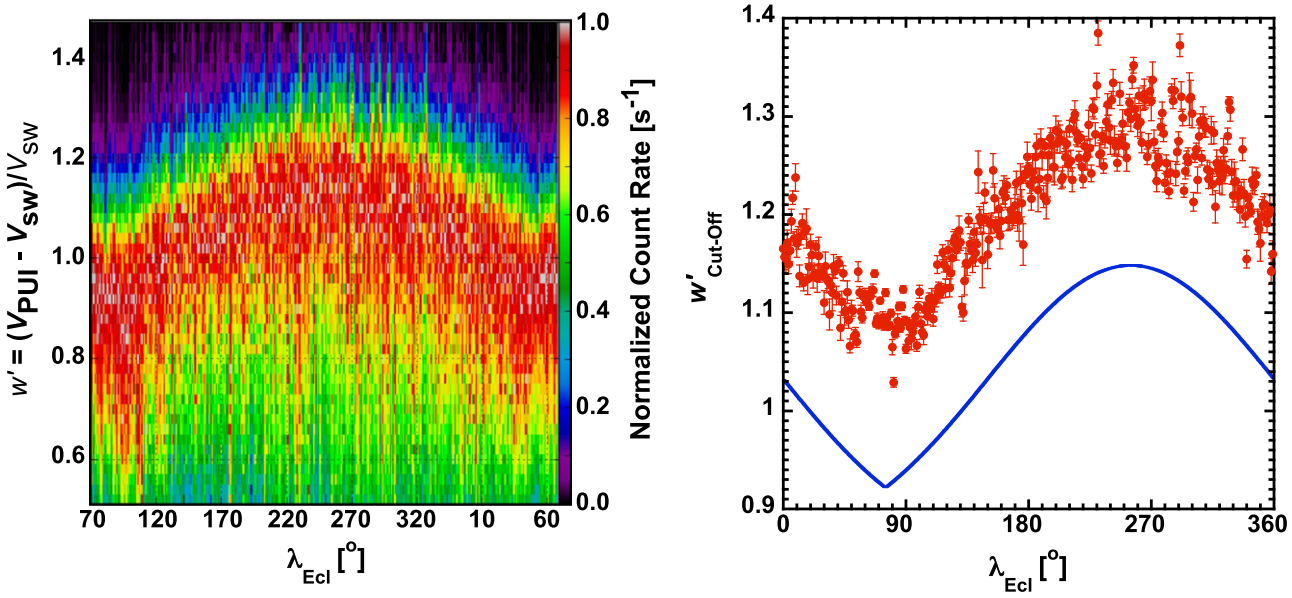

Figure 3. Left: *STEREO A* PLASTIC He^+ PUI velocity distributions in terms of accumulated counts normalized to the maximum counts in the distribution, taken along the line that connects the solar wind velocity with the center of the PUI ring-beam distribution in the plane that contains $\boldsymbol{V}_{sw}$ and $\boldsymbol{B}$ (Drews et al. 2015). Right: w'_{CutOff} in the solar wind frame obtained from the inflection point of a Tanh function as fitted to each of the individual PUI distributions on the left, along with statistical fit errors. Also shown is the model curve as obtained from Equations (1) and (5). The constant offset is likely an artifact of the simplified model, which does not take into account the exact shape of the cutoff and does not include integration over the sensor FOV and energy bands.

lead to smaller values for the cutoff value if evaluated in the spacecraft frame without consideration of the angle between the IMF $\boldsymbol{B}$ and the solar wind vector $\boldsymbol{V}_{SW}$. Also, the ring-beam distribution will not be seen in the sunward facing sector of the sensor viewing if this angle deviates from 90° by more than half the field of view (FOV) in the $\boldsymbol{B}$–$\boldsymbol{V}_{SW}$ plane.

In the following, we provide a preliminary analysis of *STEREO A* PLASTIC (Galvin et al. 2008) observations of He^+ PUIs from 2007 through 2014 restricted to time intervals with IMF conditions so that the PUI ring-beam falls into the PLASTIC FOV. We have used the unique capability of *STEREO* PLASTIC to determine the three-dimensional velocity distribution with a resolution of about 5° to obtain a radial cut through the distribution centered about the solar wind velocity vector in an angular slice that contains the ring-beam, consistent with *STEREO* IMPACT magnetic field measurements (Acuña et al. 2008). The resulting distribution transformed into the solar wind frame (w') is shown for 1° increments in ecliptic longitude λ_{Ecl} as color-coded spectra of the He^+ count rate (normalized to the maximum count rate in each 1° spectrum) in the left panel of Figure 3. For these spectra, the transformation has been performed using the aberrated solar wind as seen by a Sun orbiting spacecraft, with the V_{SW} values that were measured with PLASTIC at the 5-minute cadence of the PUI accumulation. As can be seen from the insets in Figure 2, these PUI spectra taken in the solar wind frame provide an accurate account of the PUI cutoff. The color-coded spectra mimic the expected behavior of the cutoff with ecliptic longitude. A distinct maximum is found around the previously known upwind direction relative to the ISN flow of ≈255°. The spectra exhibit some variation around the smooth trend, which is probably due to variations in the interplanetary conditions.

To obtain the cutoff values w'_{CutOff}, we have fitted the individual 1° PUI spectra (normalized count rate) shown in the left panel of Figure 3 with the function $\{1 - \mathrm{Tanh}[(w' - w'_{CutOff})/a]\}/2$. The parameter a is a scaling factor that represents the steepness of the actual cutoff slope. For the fit, count rates for $0.7 < w' < 1.5$ have been used. The resulting cutoff value w'_{CutOff} is the inflection point of the function. In the right panel of Figure 3 these cutoff values are shown as a function of λ_{Ecl}, along with the statistical fit errors and the modeled values for w'_{CutOff}, adopting $\lambda_{ISN\infty} = 75°$ as the ISN flow longitude, according to Equations (1) and (5). The observations track the model in the location of the maximum and minimum as well as in the amount of the annual variation. However, there appears to be a noticeable constant offset between the observed and modeled values of w'_{CutOff} in the amount of $\Delta w' \approx 0.15$. This offset is not too surprising because we have computed the cutoff in terms of phase space density in our model for simplicity and not the observed quantity, namely the normalized count rate, which represents the differential energy flux density of the PUI distribution. Compared with phase space density the energy flux density scales with w^4 and thus the cutoff will be flattened accordingly, pushing the inflection point to larger w values. Also, we have not attempted to reproduce the cutoff quantitatively by integrating over the sensor response function in our simplified comparison in Figure 3. The observed values of w'_{CutOff} show variations that are outside the statistical uncertainties about the trend, which by itself reflects the variation seen in the model. The fluctuations indicate systematic uncertainties in the individual data points that we will address in the discussion section. However, they appear to be distributed in ecliptic longitude in a stochastic manner so that the symmetric large-scale structure of the cutoff behavior can be exploited with the promise of much higher accuracy than these fluctuations appear to indicate.

To find the symmetry axis along the ISN flow direction, we perform a Pearson correlation analysis between results shown in the right panel of Figure 3 and their mirror distribution, where the longitude of the mirror line λ_M is varied in 1° increments, similar to the approach used by Funsten et al.

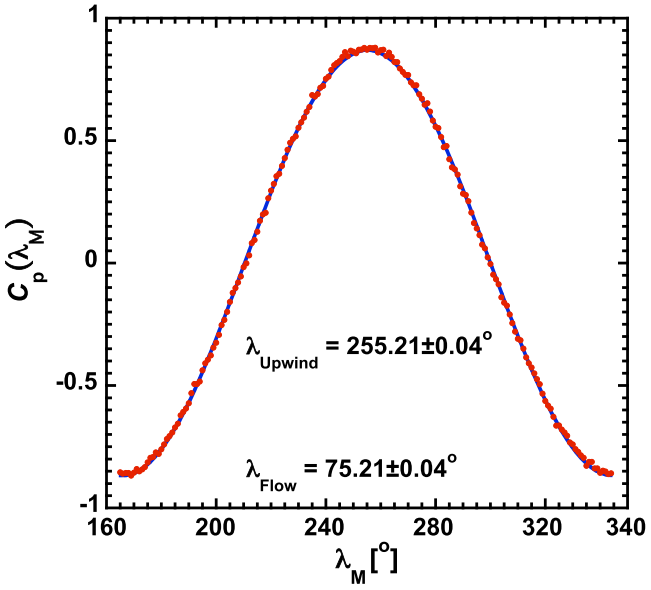

Figure 4. Pearson correlation coefficient between the observed cutoff values and those values mirror-imaged about λ_M as a function of the mirror line location λ_M. Also shown is a fit with a cosine function. The maximum correlation is associated with the symmetry line of the cutoff variation with longitude and thus represents the upwind direction of the ISN flow.

(2015) to find symmetry axes of the *IBEX* ribbon for each energy. The Pearson correlation coefficient C_p is computed for all 360 cutoff values $w'_{\mathrm{CutOff}}(\lambda_{\mathrm{Ecl}\_i})$ as

$$C_p(\lambda_M) = \frac{\sum_i \left(w'_{\mathrm{CuttOff}}(\lambda_{\mathrm{Ecl}\_i}) - w'_{\mathrm{Av}}\right)\cdot\left(w'_{\mathrm{CuttOff}}(2\lambda_M - \lambda_{\mathrm{Ecl}\_i}) - w'_{\mathrm{Av}}\right)}{\sum_i \left(w'_{\mathrm{CutOff}}(\lambda_{\mathrm{Ecl}\_i}) - w'_{\mathrm{Av}}\right)^2}, \quad (6)$$

where w'_{Av} is the average of all cutoff values. When calculating the ecliptic location angle $(2\lambda_M - \lambda_{\mathrm{Ecl}})$ for the mirrored function the result is taken modulo 360°, allowing only values between 0° and 360° for λ_{Ecl}. The resulting values of C_p are shown in Figure 4 as a function of λ_M. They vary between 0.9 and −0.9 over 180° in λ_M rather smoothly. Also shown is a fit with a cosine function, in which the amplitude and the phase were used as fit parameters. The resulting phase $\lambda_{\mathrm{Upwind}} = 255.^{\circ}21 \pm 0.^{\circ}04$ represents the upwind direction of the ISN flow, which is equivalent to the ISN flow direction $\lambda_{\mathrm{ISN}\infty} = 75.^{\circ}21 \pm 0.^{\circ}04$. The quoted uncertainty solely represents the statistical fit uncertainty and does not contain any systematic uncertainties.

4. DISCUSSION AND CONCLUSIONS

We provide an analytical model for the variation of the PUI cutoff as a function of ecliptic longitude for a given ISN flow direction at infinity. We then compare the model with *STEREO A* PLASTIC He^+ observations accumulated from 2007 through 2014. Recently, Drews et al. (2015) found that, in particular, He^+ ions injected close to 1 AU, or the ones that contribute mainly to the PUI distribution close to the cutoff, maintain the original ring-beam distribution with pitch angles according to the local IMF direction. Therefore, we restrict the data set to IMF angles close to 90° relative to the solar wind so that the ring-beam is fully within the PLASTIC FOV and thus can be analyzed in detail. By transforming the distribution into the solar wind frame we make sure that our model represents the observed cutoff values for all IMF angles under investigation. The model reflects correctly the dynamic range of the cutoff values and the shape and phasing of the variation with ecliptic longitude. The only noticeable deviation is a substantial constant offset in w' of ≈0.15. As briefly described in Section 3, we attribute this difference between model and observations mainly to the fact that, at this point, our model defines the cutoff in terms of phase space density, while we show the observations as normalized count rate, which tends to shift the cutoff in the observed direction for all PUI spectra. In addition, our model does not include quantitatively integration over the sensor FOV and energy bands. The fact that we currently use only the radial component of the ISN flow at 1 AU to determine the cutoff values cannot contribute to this constant offset. As we have discussed, this difference is one order of magnitude smaller than the variation of the cutoff over one full orbit and the radial component is identical with the full ISN velocity vector exactly upwind and downwind. However, the model represents the dynamic range of the cutoff shift and, most importantly, the phasing in longitude correctly. The determination of the ISN flow longitude, in fact, only requires obtaining the location of the maximum cutoff shift correctly, and therefore a constant offset of the values does not impact this result in any way.

To obtain the ISN flow longitude, which for obvious reasons is the symmetry line of the PUI cutoff pattern along the Earth's orbit, we have performed a Pearson correlation analysis between the observed cutoff as a function of longitude and its mirrored distribution along a chosen mirror line. The upwind direction of the ISN flow is identical with the maximum of the correlation, which exhibits a very smooth variation with longitude in spite of rather large fluctuations between the individual cutoff values. This smoothing is understandable because the correlation algorithm acts as an averaging over all 360 data points, with a comparable reduction in statistical uncertainty over the relatively larger individual error bars. As a consequence, the resulting ISN flow longitude is found with a very small statistical uncertainty $\lambda_{\mathrm{ISN}\infty} = 75.^{\circ}21 \pm 0.^{\circ}04$. This value is consistent with the most recent *IBEX* and Ulysses neutral He analyses (Bzowski et al. 2014, 2015; Leonard et al. 2015; McComas et al. 2015a, 2015b; Möbius et al. 2015b; Schwadron et al. 2015; Wood et al. 2015), which quote substantially larger statistical uncertainties and individual differences in the longitude values. While consistent with these results, our longitude value should not be taken as new measurement by itself yet, because at this point, our method still contains a number of systematic uncertainties that are likely noticeably larger than the quoted statistical uncertainty.

However, the systematic uncertainties can largely be characterized and thus eliminated from the observations. Therefore, the PUI cutoff method holds the promise to become a very high precision method to determine the ISN flow longitude, which makes it complementary to the *IBEX* observations with a narrow ISN parameter tube (McComas et al. 2012, 2015a; Möbius et al. 2015b) that will also become ever more precise with an increasing data set. We will briefly outline some of the key systematic influences that can affect the deduced flow longitude, but their complete study goes beyond the scope of this paper and is left to future investigations. One

obvious systematic effect comes from the elliptical orbit of the observing spacecraft about the Sun, while our model is based on a circular orbit. We have analyzed the expected deviation of the resulting flow longitude due to this simplification in our model and find a difference of just $0\overset{\circ}{.}05$, i.e., of the same order as the statistical uncertainty. In our data set we have used the average solar wind speed for each 1° longitude interval to adjust the observed cutoff values to the overall average $V_{\rm sw} = 337\,{\rm km\,s^{-1}}$ for the entire data set that is used in the model. While this is an appropriate initial choice, each time interval with different solar wind speed that contributes to this average should in fact be weighted with the actual PUI flux and wind speed, which may modify in particular data points that contain a wide range of solar wind speeds.

Generally, our method that is based on the cutoff is genuinely less sensitive to variations in the IMF and in wave power than other PUI methods that rely on fluxes, because PUI transport effects have not had time to alter the PUI population at the cutoff, which marks the location in the PUI distribution, where ions are freshly injected. Yet, for observations with sensors that do not provide the detailed 3D distribution of PLASTIC, such as SWICS and CTOF, IMF variations need to be taken into account. During the first year of the *STEREO* mission, *STEREO A* and *B* as well as *ACE* SWICS were co-located, which was used for cross-calibration of PUI observations (Möbius et al. 2010) and can also be used to characterize such influences. Additional unknown systematic effects can be uncovered and characterized through pair-wise comparison of annual data sets from the same spacecraft and the pair-wise comparison of data from different spacecraft, a method successfully exploited by Drews et al. (2012) in their analysis of the PUI focusing cone and crescent longitudes from He, O, and Ne PUI fluxes, because almost all such influences are stochastically distributed in longitude.

Having PUI data sets for He, O, and Ne with very good counting statistics from *SOHO* CTOF and *STEREO A* and *B* PLASTIC provides the means to tackle another potential systematic influence on the derived flow longitude that is directional in nature, i.e., small contributions of secondary He (Kubiak et al. 2014) and O contributions (Möbius et al. 2009; Park et al. 2015). As indicated in these references, the secondary populations arrive from substantially different longitudes and thus add a PUI cutoff distribution that is offset somewhat in longitude. Because of the small contribution of secondary He this is a small effect, but it may be noticeable. While He and O produce visible secondary populations via charge exchange in the outer heliosheath, the mean free path for Ne charge exchange is large compared with the size of the heliosphere and thus any secondary Ne contribution will be negligible. Therefore, a comparison between He, O, and Ne will reveal any systematic deviation due to secondary He and O components, and, at the same time, the PUI cutoff method with its potentially high precision will allow insight into the arrival direction of the secondary components in longitude and thus provide a diagnostic tool for interactions in the outer heliosheath.

In summary, we have demonstrated through a combination of analytic modeling and a correlation analysis of seven years of *STEREO A* PLASTIC observations that variation of the PUI cutoff shift with ecliptic longitude due to the ISN flow pattern along Earth's orbit can be exploited to obtain a precision determination of the interstellar flow longitude with uncertainties of the order of $0\overset{\circ}{.}1$. With $\lambda_{\rm ISN\infty} = 75\overset{\circ}{.}21 \pm 0\overset{\circ}{.}04$, the preliminary analysis presented here provides a result that is consistent with recent analyses of direct ISN He observations by *IBEX* and *Ulysses* and the assumption that the ISN flow direction has not changed from the beginning of the Ulysses observations until now within the combined uncertainties of all these measurements. However, it should be reemphasized that the uncertainty quoted for the PUI result thus far is solely statistical in nature, and all systematic uncertainties must be evaluated comprehensively. But the still needed analysis of systematic uncertainties is very promising. In particular, key processes that influence related studies using PUI fluxes, such as ionization rates and PUI transport effects, are at most of minor importance for the PUI cutoff.

With *ACE* SWICS, *SOHO* CTOF, and *STEREO A* and *B* PLASTIC, PUI data are available that span more than 18 years and provide simultaneous coverage at different ecliptic longitudes. Given the very small statistical uncertainty, the PUI cutoff method presented here, once fully evaluated, holds the promise to become sensitive to sub-degree variations in the ISN flow direction, if they exist, or will provide very tight upper limits. *STEREO* and *SOHO* observations also allow the study of He, O, and Ne PUIs with good counting statistics. These multi-species observations will provide insight into deflection of the interstellar flow in the outer heliosheath and, at the same time allow us to assess the influence of secondary neutrals in the O and He distribution in our determination of the flow longitude, because for Ne no secondary population is expected.

This work was supported by NASA through the *Advanced Composition Explorer* (*ACE*) under NNX08AI11G, *Interstellar Boundary Explorer* (*IBEX*) under NNG05EC85C, and *STEREO* under NNX13AP52G, and under DFG (Wi2139/7-1) and DLR (50 0C 1103) at the Universität Kiel. M. Lee's work was also supported under SR&T Grant NNX12AB32G and LWS Grant NNX11AO97G.

REFERENCES

Acuña, M., Curtis, D., Scheifele, J. L., et al. 2008, SSRv, 136, 203
Adams, T. F., & Frisch, P. C. 1977, ApJ, 212, 300
Ajello, J. M. 1978, ApJ, 222, 1068
Bertaux, J., & Blamont, J. 1971, A&A, 11, 200
Bochsler, P., Petersen, L., Möbius, E., et al. 2012, ApJS, 198, 13
Bzowski, M., Kubiak, M., Hłond, M., et al. 2014, A&A, 569, A8
Bzowski, M., Kubiak, M. A., Möbius, E., et al. 2012, ApJS, 198, 12
Bzowski, M., Swaczyna, P., Kubiak, M. A., et al. 2015, ApJS, 220, 28
Chalov, S. 2014, MNRAS Lett., 443, L25
Chalov, S., & Fahr, H.-J. 2006, AstL, 32, 487
Drews, C., Berger, L., Taut, A., et al. 2015, A&A, 575, A97
Drews, C., Berger, L., Wimmer-Schweingruber, R. F., et al. 2012, JGR, 117, 9106
Frisch, P. C., Bzowski, M., Drews, C., et al. 2015, ApJ, 801, 61
Frisch, P. C., Bzowski, M., Livadiotis, G., et al. 2013, Sci, 341, 1080
Funsten, H. O., Cai, D. M., Dayeh, M., et al. 2015, ApJ, 799, 68
Galvin, A. B., Kistler, L. M., Popecki, M. A., et al. 2008, SSRv, 136, 437
Gloeckler, G., Geiss, J., Balsiger, H., et al. 1992, A&A, 92, 267
Gloeckler, G., Möbius, E., Geiss, J., et al. 2004, A&A, 426, 845
Gloeckler, G., Schwadron, N. A., Fisk, L. A., & Geiss, J. 1995, GeoRL, 22, 2665
Kubiak, M. A., Bzowski, M., Sokół, J. M., et al. 2014, ApJ, 213, 29
Lallement, R., & Bertaux, J.-L. 2014, A&A, 565, A41
Lallement, R., Raymond, J. C., Vallerga, J., et al. 2004, A&A, 426, 875
Lee, M. A., Kucharek, H., Möbius, E., et al. 2012, ApJS, 198, 13
Lee, M. A., Leonard, T., & Möbius, E. 2015, ApJS, 220, 23
Leonard, T., Möbius, E., Bzowski, M., et al. 2015, ApJ, 804, 42
McComas, D. J., Bzowski, M., Fahr, H., et al. 2012, Sci, 336, 1291
McComas, D. J., Bzowski, M., Frisch, P. C., et al. 2015a, ApJ, 802, 28

McComas, D. J., Bzowski, M., Galli, A., et al. 2015b, ApJS, 220, 22
Möbius, E., Bochsler, P., Bzowski, M., et al. 2009, Sci, 326, 969
Möbius, E., Bochsler, P., Bzowski, M., et al. 2012, ApJS, 198, 11
Möbius, E., Bzowski, M., Chalov, S., et al. 2004, A&A, 426, 897
Möbius, E., Bzowski, M., Frisch, P. C., et al. 2015b, ApJS, 220, 24
Möbius, E., Bzowski, M., Fuselier, S. A., et al. 2015a, in AIP Conf Proc. 577, J. Phys., Conf. Ser. 012019, Voyager, IBEX, and the Interstellar Medium (Bristol: IOPP)
Möbius, E., Hovestadt, D., Klecker, B., Scholer, M., & Gloeckler, G. 1985, Natur, 318, 426
Möbius, E., Klecker, B., Bochsler, P., et al. 2010, in AIP Conf. Proc. 1302, Pickup Ions Throughout the Heliosphere and Beyond (Melville, NY: AIP), 37
Möbius, E., Litvinenko, Y., Grünwaldt, H., et al. 1999, GeoRL, 26, 3181
Möbius, E., Rucinski, D., Hovestadt, D., & Klecker, B. 1995, A&A, 304, 505
Möbius, E., Rucinski, D., Isenberg, P. A., & Lee, M. A. 1996, AnGeo, 14, 492
Möbius, E., Rucinski, D., Lee, M. A., & Isenberg, P. A. 1998, JGR, 102, 257
Oka, M., Terasawa, T., Noda, H., Saito, Y., & Mukai, T. 2002, GeoRL, 29, 1612
Opher, M., Stone, E. C., & Gombosi, T. 2007, Sci, 316, 875
Park, J., Kucharek, H., Möbius, E., et al. 2015, ApJS, 220, 34
Pogorelov, N. V., Heerikhuisen, J., Mitchell, J. J., Cairns, I. H., & Zank, G. P. 2009, ApJL, 695, 31
Saul, L., Wurz, P., Rodriguez, D., et al. 2012, ApJS, 198, 14
Schwadron, N. A., Adams, F. C., Christian, E., et al. 2014, Sci, 343, 988
Schwadron, N. A., Möbius, E., Fuselier, S. A., et al. 2015, ApJS, 220, 25
Sokół, J., & Bzowski, M. 2014, arXiv:1411.4826
Thomas, G. E., & Krassa, R. F. 1971, A&A, 11, 218
Weller, C., & Meier, R. 1974, ApJ, 193, 471
Witte, M. 2004, A&A, 426, 835
Witte, M., Banaszkiewicz, M., & Rosenbauer, H. 1996, SSRv, 78, 289
Wood, B., Mueller, H.-R., & Witte, M. 2015, ApJ, 801, 62